Supplementary Information (SI) for Journal of Materials Chemistry A.
This journal is © The Royal Society of Chemistry 2026

Supporting Information for:

Carboxylated CNT–Vanadium Hexacyanoferrate Cathode Enabling High-Energy-Density Quasi-Solid-State H_2 Batteries with Enhanced Low-Temperature Performance

Experimental Section

Preparation of the BP electrolyte:

BP was prepared by ball milling 4 g of hydrophilic bentonite at 500 rpm for 1 h, followed by mixing with 63 wt% H_3PO_4 at a weight ratio of 1:1.4 in a 5 mL beaker to form a gel, denoted as BP, which serves as a proton-conducting quasi-solid-state clay/acid composite electrolyte that is mechanically self-supporting and non-flowing under the operating conditions.

First principles calculations:

All calculations in this study were performed with the Vienna ab initio Simulation Package (VASP)[1] within the frame of density functional theory (DFT). The exchange-correlation interactions of electron were described via the generalized gradient approximation (GGA) with PBE functional[2], and the projector augmented wave (PAW) method[3] was used to describe the interactions of electron and ion. Additionally, the DFT-D3 method[4-5] was used to account for the long-range van der Waals forces present within the system. The Monkhorst-Pack scheme was used for the integration in the irreducible Brillouin zone. The kinetic energy cut-off of 450 eV was chosen for the plane wave expansion. The lattice parameters and ionic position were fully relaxed, and the total energy was converged within 10^{-5} eV per formula unit. The final forces on all ions are less than 0.02/Å. The spin polarized effect was included in all calculations above. The migration of H was calculated use the CI-NEB method. Structural model used was based on the orthogonal cell of CC-VHCF with the lattice parameters of a = 20.33 Å b=10.16 Å c=10.16 Å, the carboxyl groups were placed randomly in the cell.

Electrochemical measurements:

Half-cell testing was conducted in Swagelok-type cells; the configuration comprised a CC-VHCF working electrode, a self-supporting carbon counter electrode, and an Ag/AgCl reference electrode. Full-cell tests were performed with CC-VHCF as the cathode and hydrogen (H_2) as the anode, with a BP (bentonite–phosphoric acid) as the quasi-solid-state electrolyte. Cyclic voltammetry (CV) and electrochemical impedance spectroscopy (EIS) were conducted

on a CHI760E electrochemical workstation (Shanghai Chenhua, China), and galvanostatic charge–discharge (GCD) measurements were carried out using a LAND CT3004K battery testing system (Wuhan LAND, China). The low-temperature performance of the whole battery was tested on low-temperature test chambers (DW-86L630). For ex situ FTIR analysis and ex-situ XPS analysis, the active material was gently scraped from the electrode surface after charging or discharging and collected for measurement.

Potential conversion to the RHE scale:

All potentials measured versus the Ag/AgCl (saturated KCl) reference electrode in the half-cell tests were converted to the RHE scale according to E(RHE) = E(Ag/AgCl) + 0.197 V + 0.0591 × pH (at 25 °C). The electrolyte used was 63 wt% H_3PO_4, and all measurements were conducted at 25 °C.

Calculation of energy and power densities:

The energy density and power density were calculated from the galvanostatic discharge curves and normalized to the mass of the cathode active material.

The gravimetric energy density in this work was calculated according to:

$$Energy\ density\ (Wh\ kg-1) = \frac{discharge\ capacity\ (mAh) \times average\ discharge\ voltage\ (V)}{mass(g)}$$

and the gravimetric power density was calculated according to:

$$Energy\ density\ (Wh\ kg-1) = \frac{discharge\ \text{current}\ (mA) \times average\ discharge\ voltage\ (V)}{mass(g)}$$

Here, the mass refers to the mass of the cathode active material. Therefore, unless otherwise specified, all the reported energy and power density values in this work are based on the mass of the cathode active material.

Determination of apparent activation energy:

The apparent activation energy was obtained by Arrhenius fitting of the temperature-dependent electrochemical impedance spectroscopy (EIS) data measured in a half-cell configuration. The cathode material was used as the working electrode, activated carbon as the counter electrode, Ag/AgCl as the reference electrode, and 63 wt% H_3PO_4 as the electrolyte. Therefore, the derived

activation energy reflects an apparent proton-transport parameter of the practical half-cell system, which may include contributions from proton transport in the cathode, the electrode/electrolyte interface, and the proton-rich electrolyte environment, rather than the intrinsic local migration barrier of an idealized solid-state model.

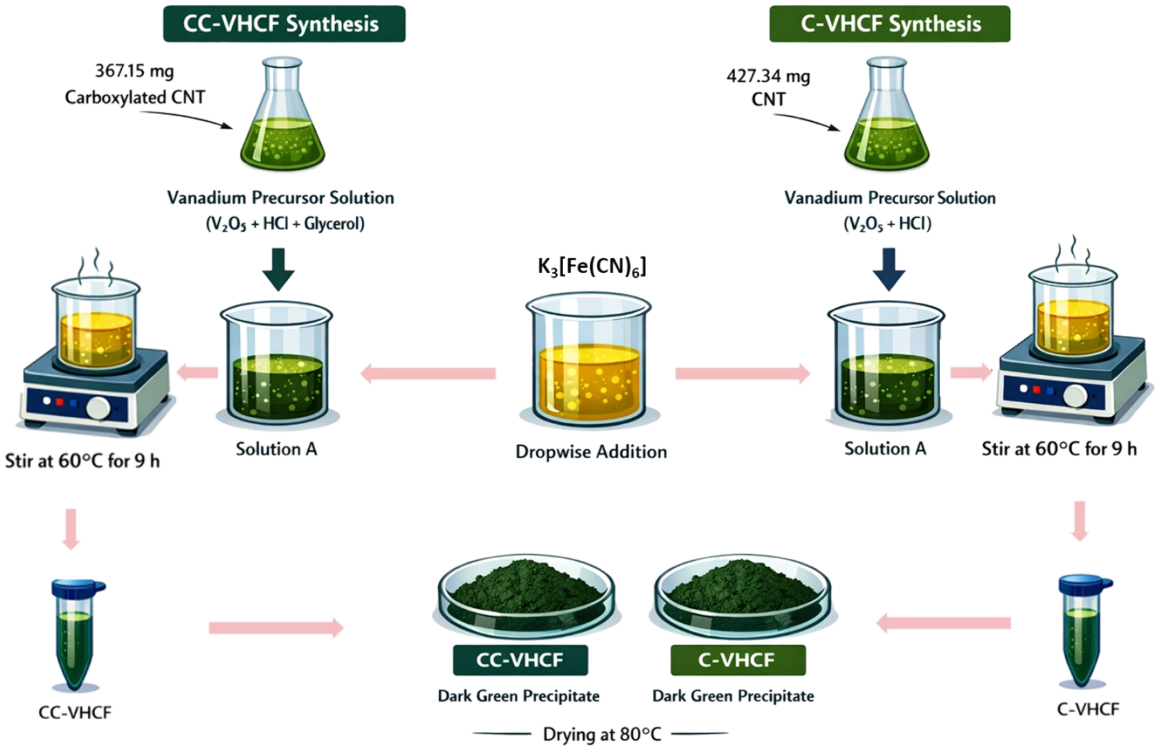

Fig. S1 Schematic synthesis routes of CC-VHCF and C-VHCF.

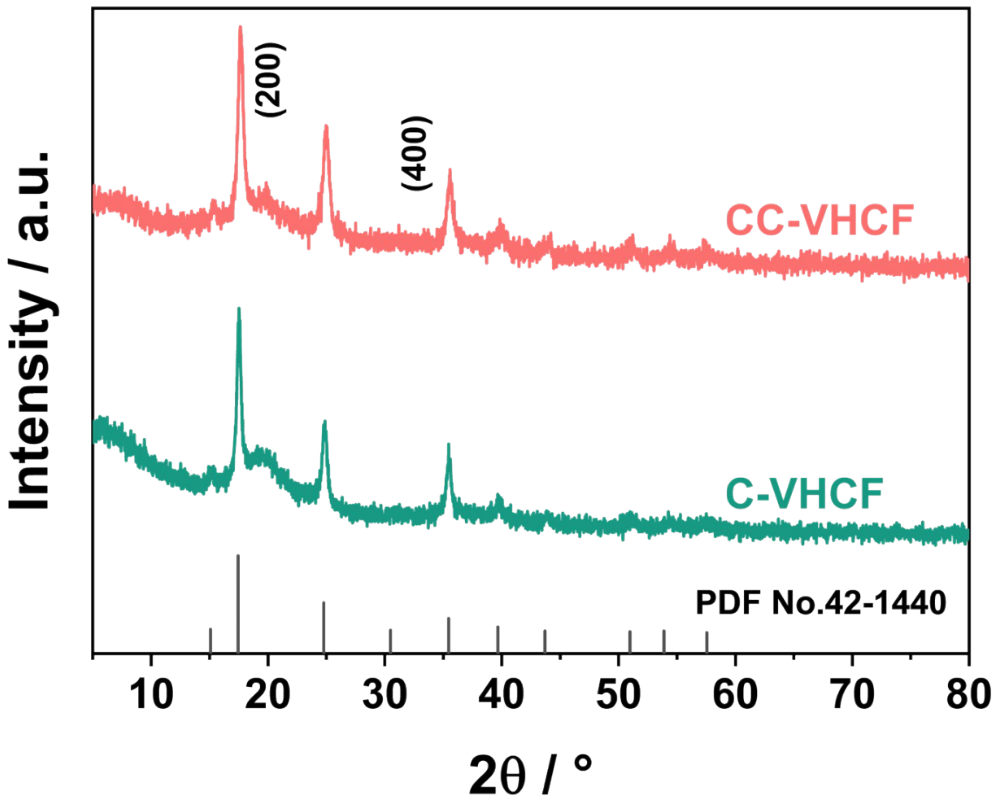

Fig. S2 XRD patterns of CC-VHCF and C-VHCF.

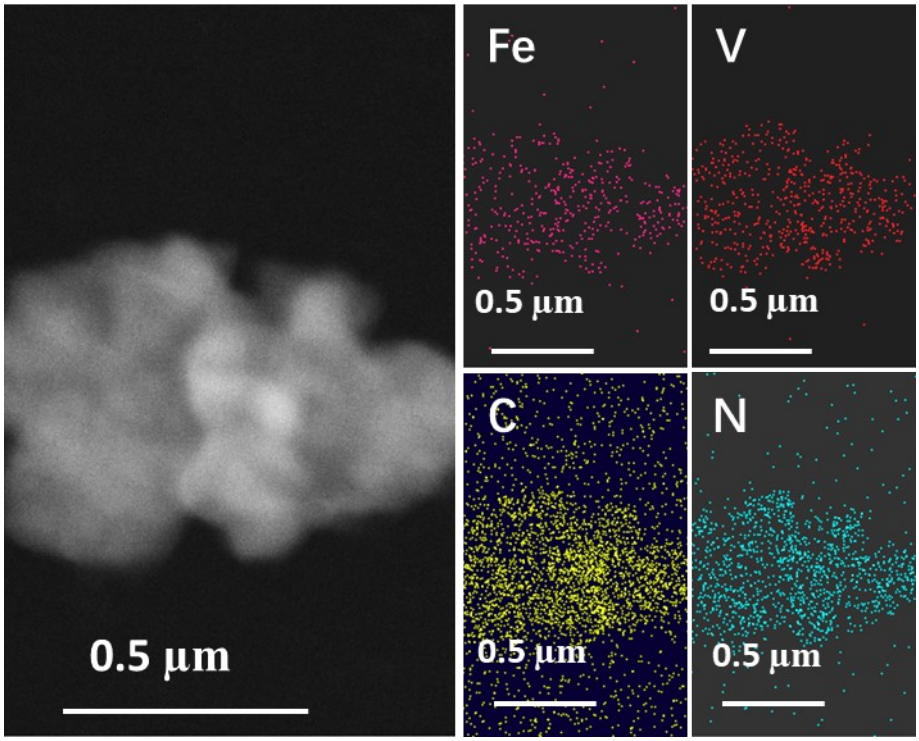

Fig. S3 TEM and EDS-mapping images of C-VHCF.

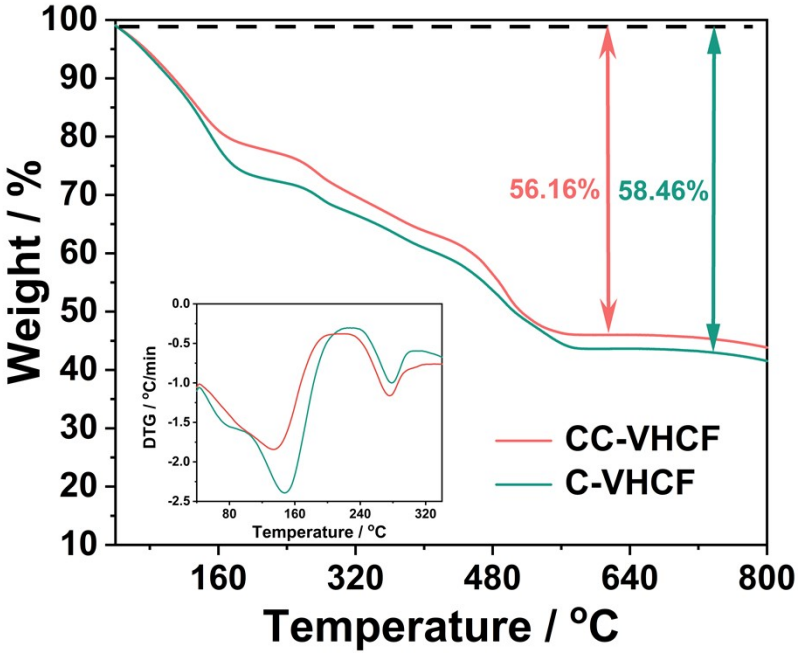

Fig. S4 TGA curves of CC-VHCF and C-VHCF are shown (inset: corresponding derivative curves).

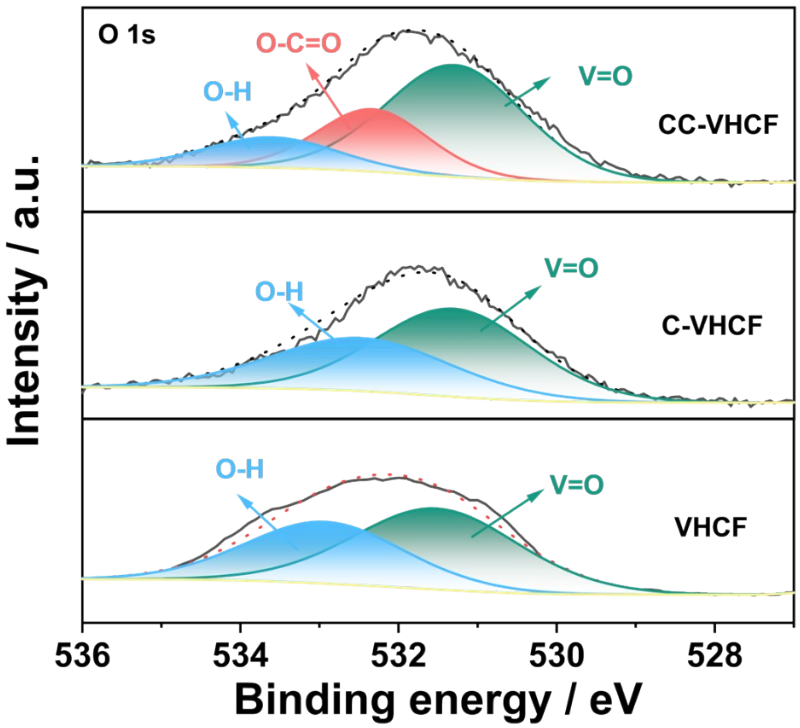

Fig. S5 XPS spectra of O 1s for different samples.

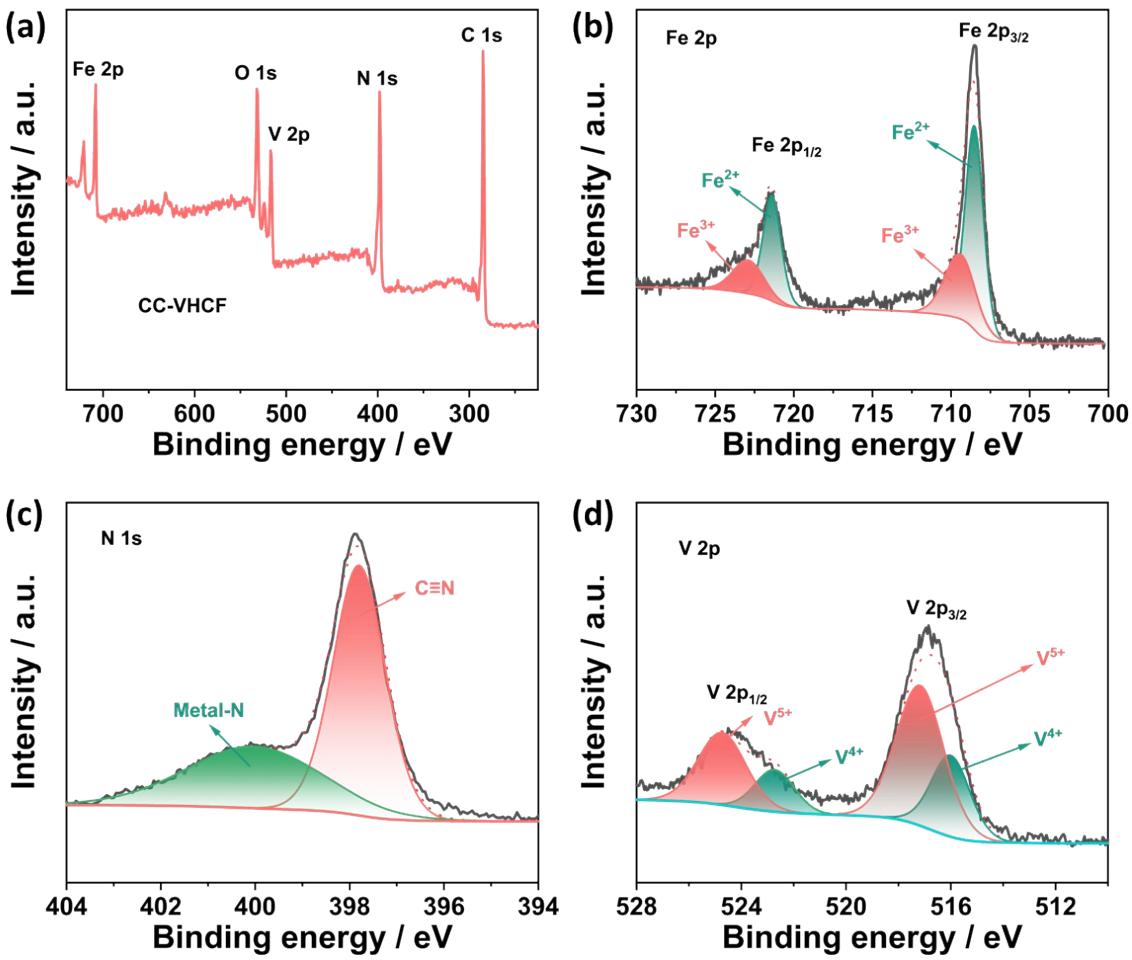

Fig. S6 XPS spectra of (a) CC-VHCF (b) Fe 2p, (c) N1s, and (d) V 2p.

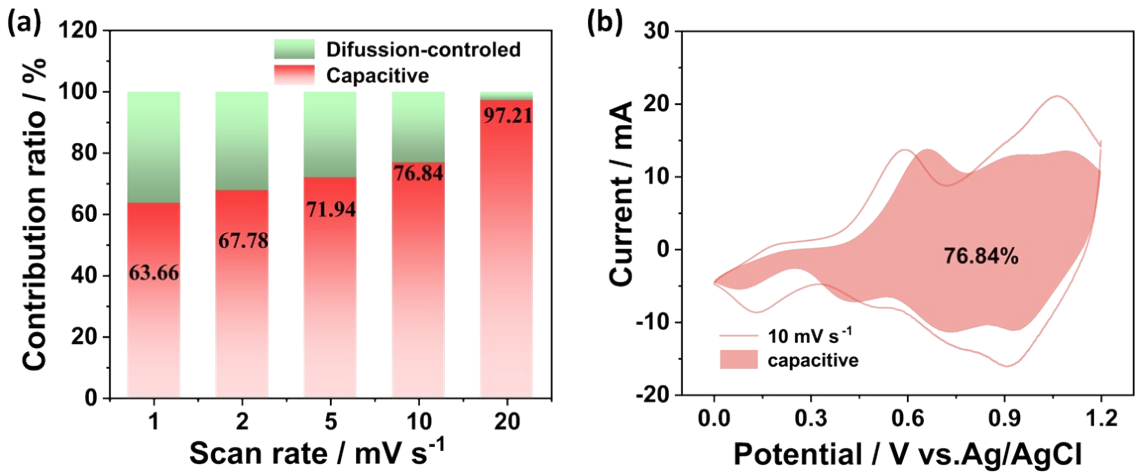

Fig. S7 (a) Capacity and diffusion control contributions ratios at different scan rates. (b) Plot of capacitive charge storage contribution to the total capacity at a scan rate of 10 mV s^{-1}.

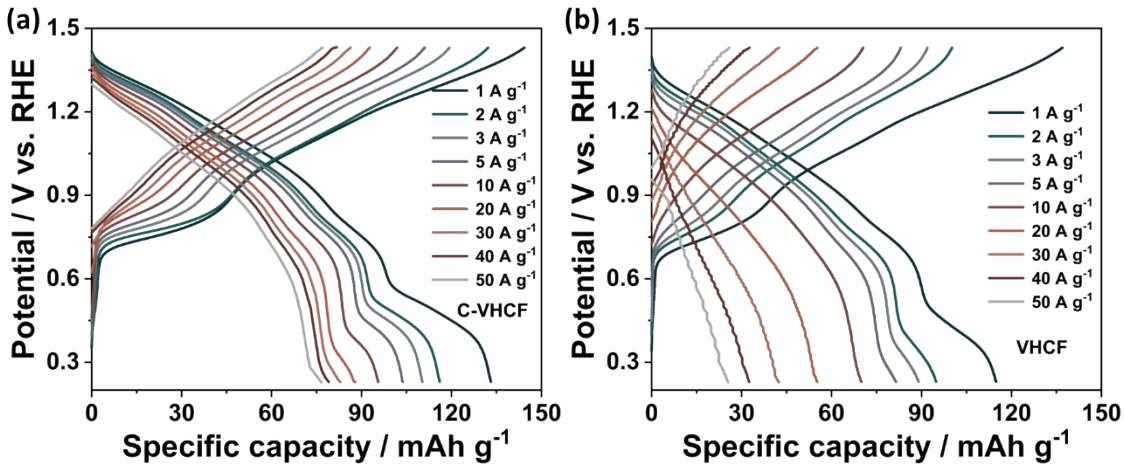

Fig. S8 GCD curves of C-VHCF and VHCF.

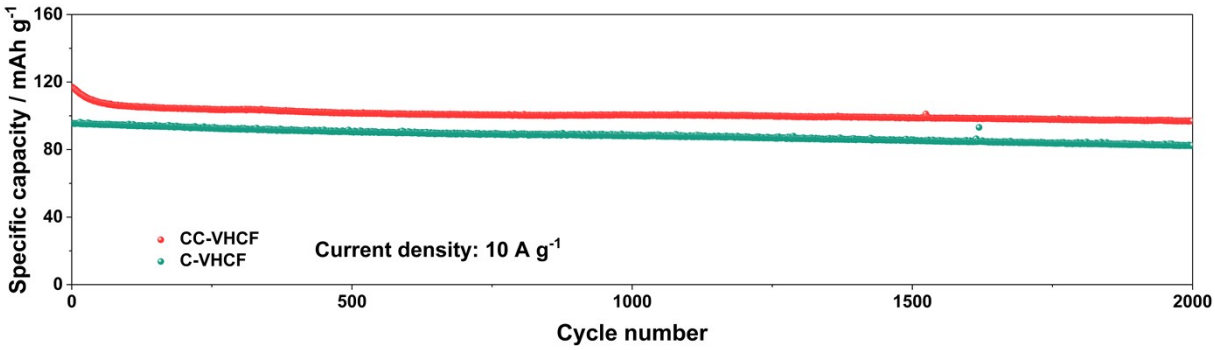

Fig. S9 Cycling performance of CC-VHCF and C-VHCF at 10 A g^{-1}.

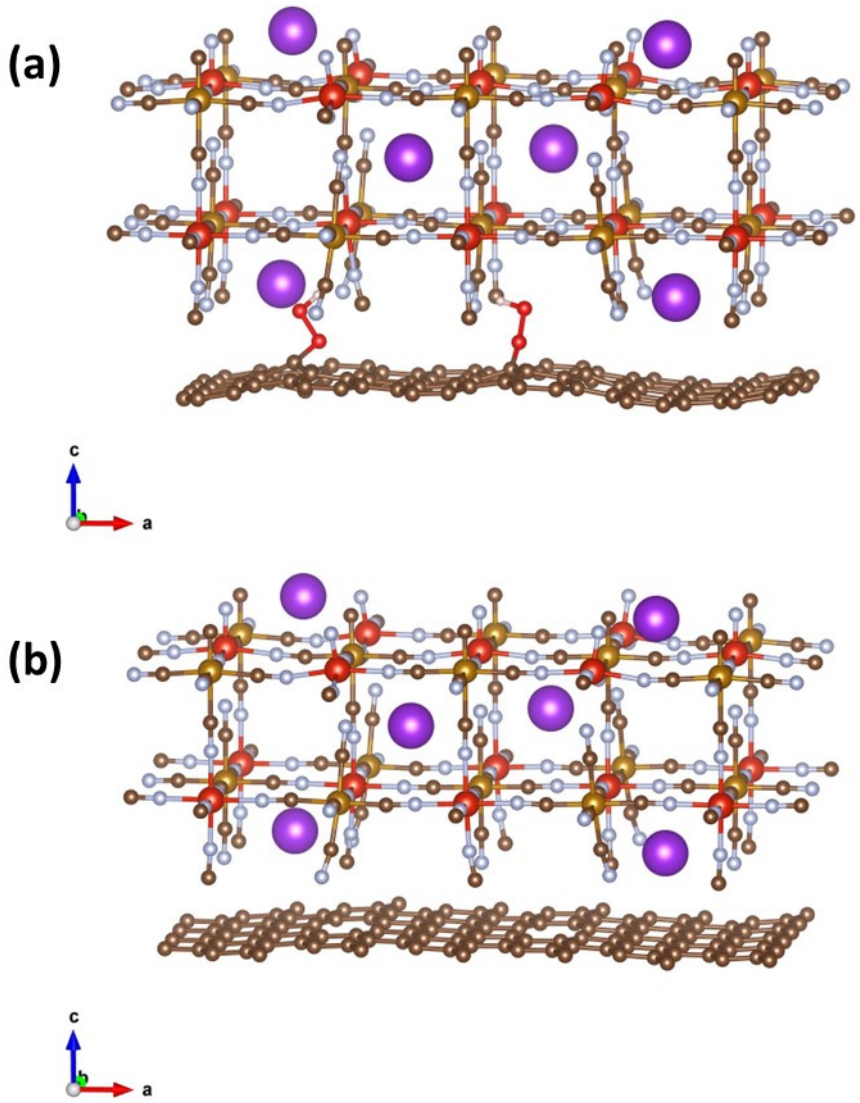

Fig. S10 Model diagram of H^+ migration barrier calculation of (a) CC-VHCF and (b) C-VHCF.

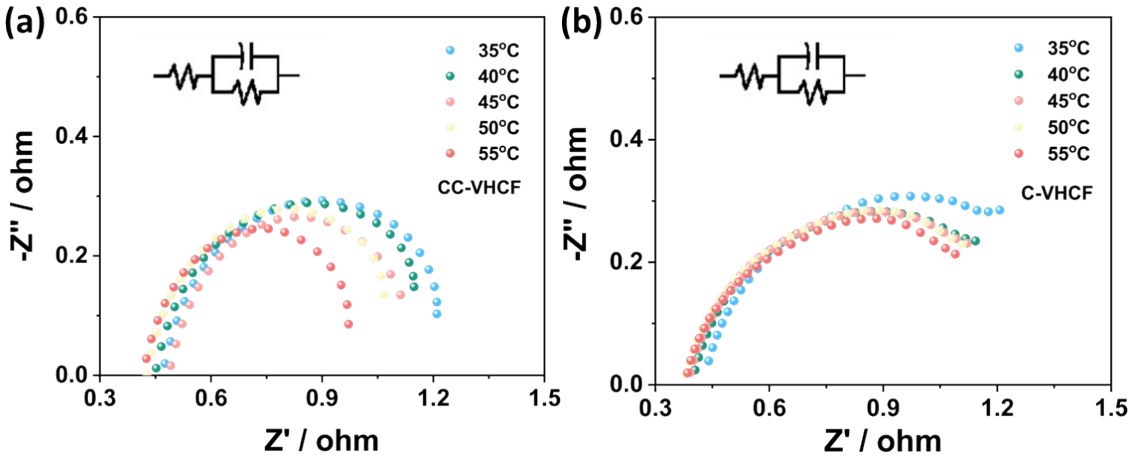

Fig. S11 EIS of (a) CC-VHCF and (b) C-VHCF (inset shows the equivalent circuit diagram).

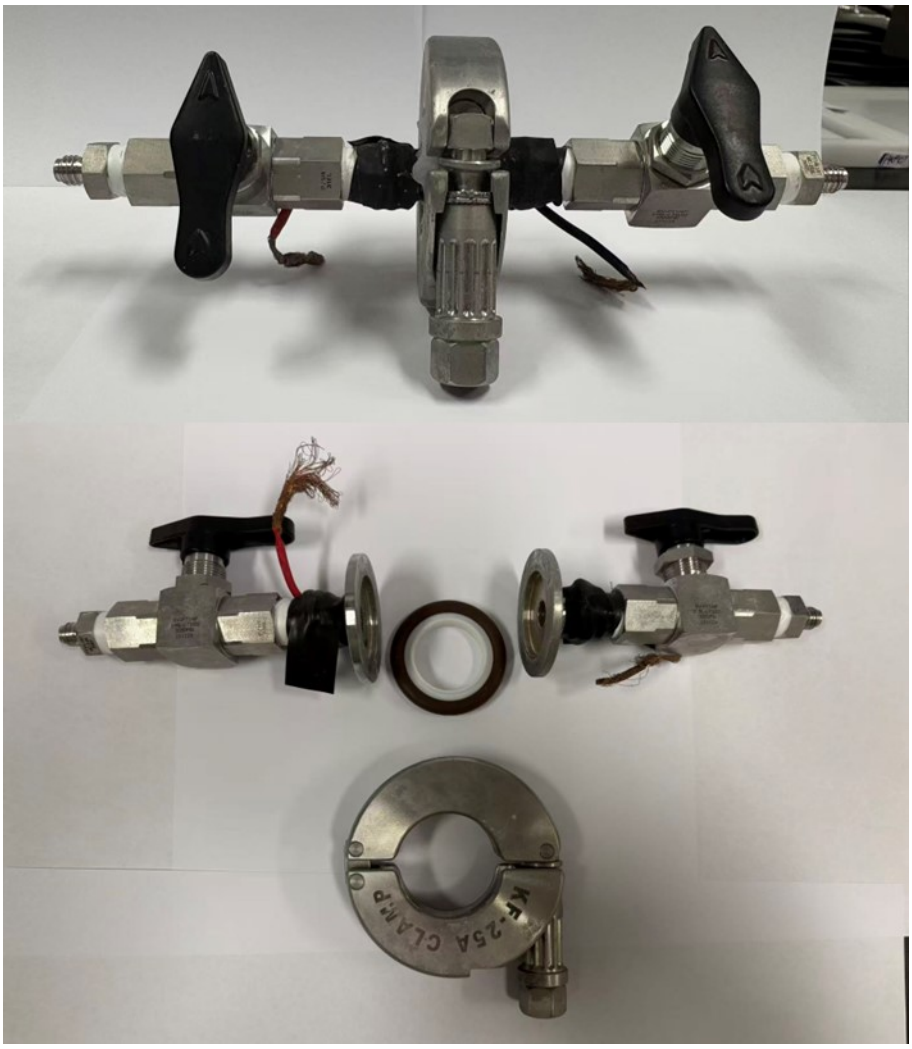

Fig. S12 Prototypical quasi-solid-state H_2/CC-VHCF gas battery, consisting of a CC-VHCF cathode, a BP quasi-solid-state electrolyte, and a Pt/H_2 anode in a button-cell-type configuration.

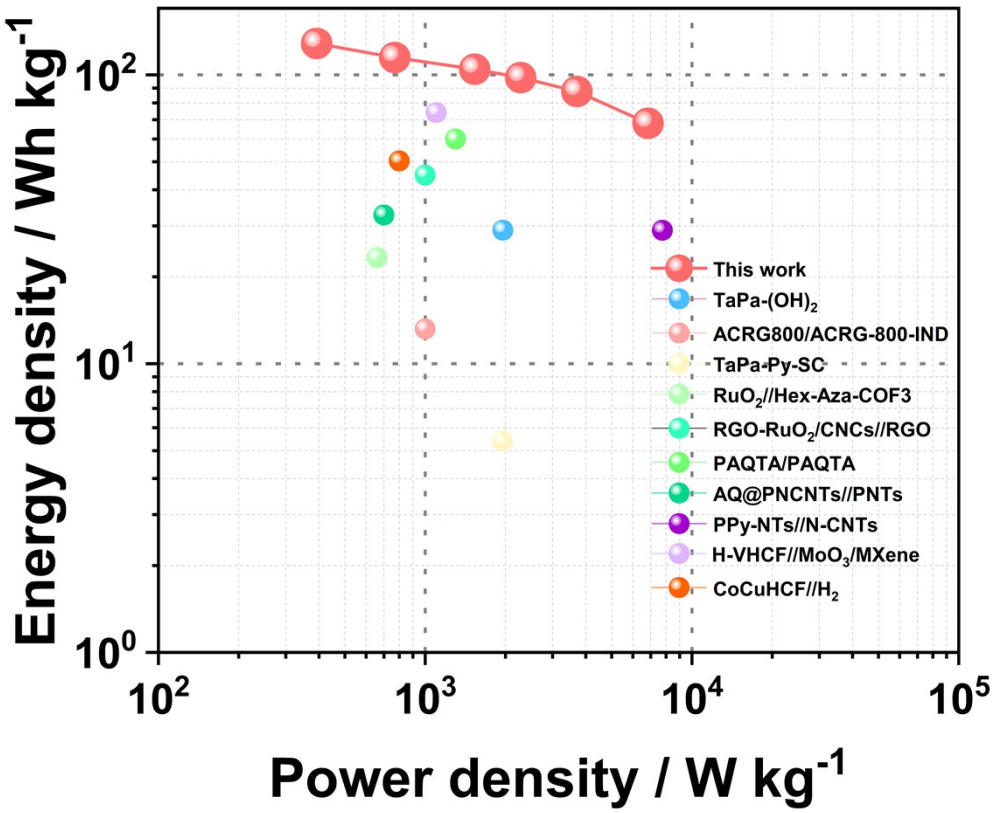

Fig. S13 Ragone plot of the quasi-solid-state H_2/CC-VHCF gas battery measured at room temperature. The energy and power densities were calculated from the galvanostatic discharge curves and normalized to the mass of the cathode active material. Literature values were taken from the corresponding references and compared on the basis reported in the original publications.

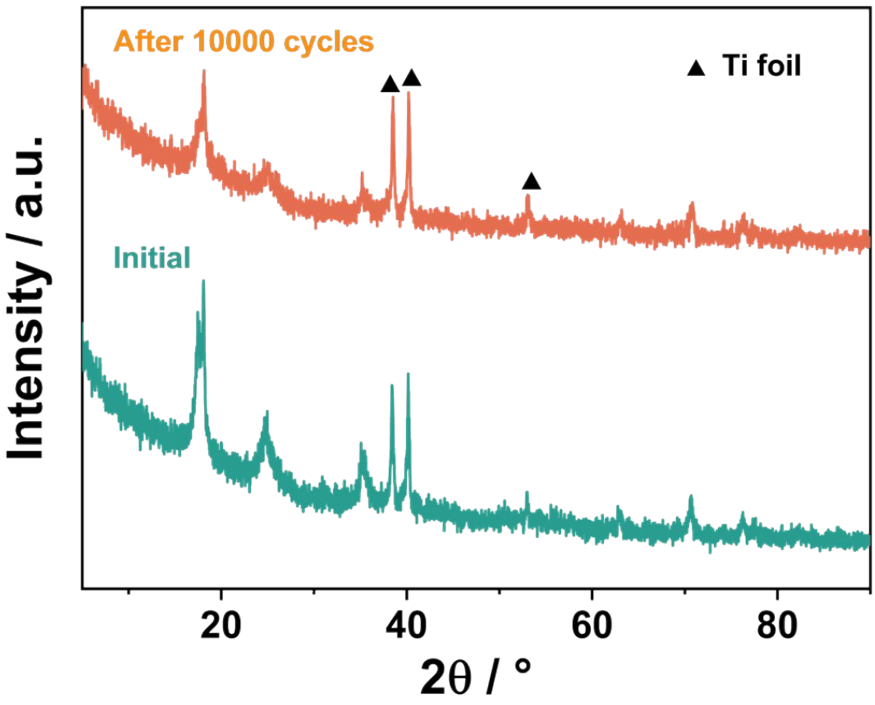

Fig. S14 Ex situ XRD patterns of the initial and cycled CC-VHCF cathodes after 10,000 cycles.

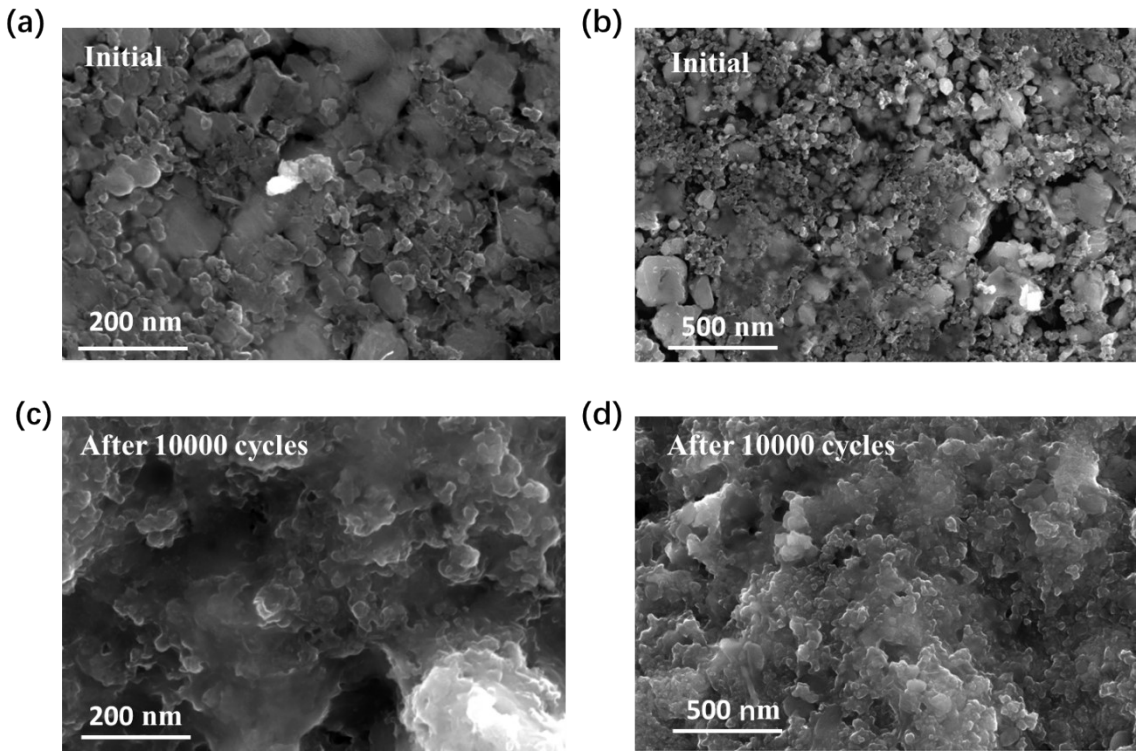

Fig. S15 SEM images of the initial and cycled CC-VHCF cathodes after 10,000 cycles.

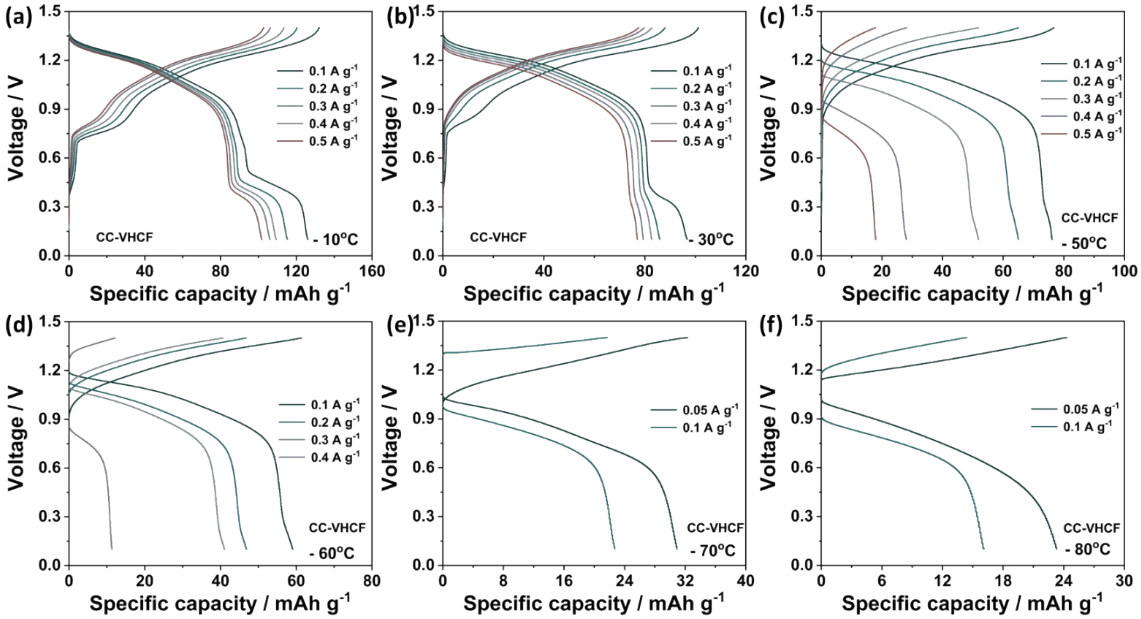

Fig. S16 Rate performance of the quasi-solid-state H_2/CC-VHCF gas battery at different temperatures: (a) −10 °C, (b) −30 °C, (c) −50 °C, (d) −60 °C, (e) −70 °C and (f) −80 °C. The device uses a CC-VHCF cathode, a BP quasi-solid-state electrolyte, and a Pt/H_2 anode.

Table S1. Comparison of CC-VHCF electrodes with others based on proton system.

System	Voltage (V) 25°C	Specific capacity (mAh g^{-1})	Temperature (°C)	Rate (current density) 25 °C	References
MnO_2//2 M $AlCl_3$/Nafion 117/2 M $MnSO_4$// Al-MoO_x	1-1.9	145		0.17-13.33 A g^{-1}	6
MnO_2 //1 M H_2SO_4+1 M $MnSO_4$// MoO_3@TiO_2	0.8-1.6	200.8		1-20 A g^{-1}	7
MnO_2//2 M H_2SO_4+2 M $MnSO_4$// MoO_3	0.85-1.55	190	-70	1-60 A g^{-1}	8
MnO_2@GF//2 M H_2SO_4+2 M $MnSO_4$//PTO	0.3-1.3	210	-70-25	0.16-400 mA cm^2	9
MnO_2@GF//2 M HBF_4+2 M Mn $(BF_4)_2$// MoO_3	0.4-1.4	150	-90-25	5-25 A g^{-1}	10
CuFe-TBA// AiCE//MoO_3	0-1.5	33	-20-25	0.05-16 A g^{-1}	11
NAC//1 M H_2SO_4//MoO_3 NBS	0-1.6	57.8	-25-65	1-20 A g^{-1}	12
VHCF//9.5 M H_3PO_4//MoO_3@MXene	0-1.5	73	-40-25	1-50 A g^{-1}	13

H-TBA//1 M H_2SO_4//MoO_3	0-1.6	51		2.5-50 A g^{-1}	14
$LiVPO_4F$// PPA//MoO_3	0-1.3	55	0-100	0.093-0.186 A g^{-1}	15
HDC//1 M H_2SO_4//AC	-0.3-0.7	50		0.1-1 A g^{-1}	16
CuFe-TBA//1 M H_2SO_4// CuC_2O_x	0-0.7	42		0.1-3 A g^{-1}	17
HVFe-PBA// SSAE//MoO_3	0.1-1.8	105	-60-40	0.5-100 A g^{-1}	18
CoCuHCF//H6D1 7.5 M H_3PO_4//H_2	0.2-1.3	51.7	-80-25	5-50 A g^{-1}	19
CuHCF//9 M H_3PO_4//H_2	0.5-1.2	48.3	-80-25	0.5-48 A g^{-1}	20
$LiVPO_4F$//BP//H_2	0.2-1.2	62.3		0.1-1 A g^{-1}	21
CC-VHCF//BP//H_2	**0.1-1.4**	**163.7**	**-80-25**	**0.5-30 A g^{-1}**	**This work**

Table S2. The energy and power densities of quasi-solid-state H_2/CC-VHCF gas battery compared to other batteries.

Systems	Electrolytes	Energy densities (Wh kg^{-1})	Power densities (kW kg^{-1})	Ref.
TpPa-$(OH)_2$	1 M phosphate buffer	29	1.956	22
ACRG-800/ACRG-800-IND	1 M H_2SO_4	13.2	1	23
TaPa-Py-SC	1 M H_2SO_4	5.4	1.95	24
RuO_2//Hex-Aza-COF3	1 M H_2SO_4	23.3	0.661	25
RGO-(RuO_2/CNCs)//RGO	30 wt% KOH	45	1	26
PAQTA/PAQTA	0.5 M H_2SO_4	60	1.3	27
AQ@PNCNTs//PNTs	1 M H_2SO_4	32.7	0.7	28
PPy-NTs//N-CNTs	1 M H_2SO_4	28.95	7.75	29
H-VHCF// MoO_3/MXene	9.5 M H_3PO_4	75	1.1	13
CoCuHCF//H_2	H6D1-7.5 M H_3PO_4	50.4	0.8	19
CC-VHCF//H_2	BP	128.5	0.392	This work

Table S3. Comparison of quasi-solid-state H_2/CC-VHCF gas battery with other batteries in terms of operating temperature, specific capacity, cycling performance, and current density.

System	Temperature (°C)	Specific capacity (mAh g^{-1})	Cycle number	current density (A g^{-1})	References
CuFe-TBA// AiCE//MoO_3	-35	23.8	500	0.05 A g^{-1}	11
NAC//1 M H_2SO_4//MoO_3 NBS	-25	42.7	0	1 A g^{-1}	12
VHCF//8.5 M H_3PO_4//MoO_3@MXene	-40	32	10000	0.5 A g^{-1}	13
$LiVPO_4F$// PPA//MoO_3	-10	10	0	0.025 A g^{-1}	15
HVFe-PBA// SSAE//MoO_3	-60	32.4	5500	1 A g^{-1}	18
CoCuHCF//H6D1 7.5 M H_3PO_4//H_2	-50	41.2	1000	0.1 A g^{-1}	19
CuHCF//9 M H_3PO_4//H_2	-60	34	1150	0.025 A g^{-1}	20
CC-VHCF//BP//H_2	-40	75.5	1000	0.3 A g^{-1}	This work

References

[1] J. P. Perdew, K. Burke and M. Ernzerhof, *Phys. Rev. Lett.*, 1996, **77**, 3865–3868.
[2] G. Kresse and D. Joubert, *Phys. Rev. B*, 1999, **59**, 1758–1775.
[3] S. Grimme, J. Antony, S. Ehrlich and H. Krieg, *J. Chem. Phys.*, 2010, **132**, 154104.
[4] S. Grimme, S. Ehrlich and L. Goerigk, *J. Comput. Chem.*, 2011, **32**, 1456–1465.
[5] H. J. Monkhorst and J. D. Pack, *Phys. Rev. B*, 1976, **13**, 5188–5192.
[6] Liu, H.; Cai, X.; Zhi, X.; Di, S.; Zhai, B.; Li, H.; Wang, S.; Li, L. An Amorphous Anode for Proton Battery. *Nano-Micro Lett.* 2023, **15**, 24.
[7] C.-G. Wang, S.-S. Zhao, X.-X. Song, N.-N. Wang, H.-L. Peng, J. Su, S.-Y. Zeng, X.-J. Xu and J. Yang, *Adv. Energy Mater.*, 2022, **12**, 2200157.
[8] L. Yan, J.-H. Huang, Z.-W. Guo, X.-L. Dong, Z. Wang and Y.-G. Wang, *ACS Energy Lett.*, 2020, **5**, 685–691.
[9] Z. Guo, J.-H. Huang, X.-L. Dong, Y. Xia, L. Yan, Z. Wang and Y.-G. Wang, *Nat. Commun.*, 2020, **11**, 959.
[10] T. Sun, H. Du, S. Zheng, J. Shi and Z. Tao, *Adv. Funct. Mater.*, 2021, **31**, 2010127.
[11] S. Wang, H. Jiang, Y. Dong, D. Clarkson, H. Zhu, C. M. Settens, Y. Ren, T. Nguyen, F. Han, W. Fan, S. Y. Kim, J. Zhang, W. Xue, S. K. Sandstrom, G. Xu, E. Tekoglu, M. Li, S. Deng, Q. Liu, S. G. Greenbaum, X. Ji, T. Gao and J. Li, *Adv. Mater.*, 2022, **34**, 2202063.
[12] Y. Wu, W. Liu, Z. Zhang, Y. Zheng, X. Fu, J. Lu, S. Cheng, J. Su and Y. Gao, *Energy Storage Mater.*, 2023, **61**, 102849.
[13] X. Dong, Z. Li, D. Luo, K. Huang, H. Dou and X. Zhang, *Adv. Funct. Mater.*, 2023, **33**, 2210473.
[14] X. Wang, Y. Xie, K. Tang, C. Wang and C. Yan, *Angew. Chem., Int. Ed.*, 2018, **57**, 11569–11573.
[15] M. Liao, X. Ji, Y. Cao, J. Xu, X. Qiu, Y. Xie, F. Wang, C. Wang and Y. Xia, *Nat. Commun.*, 2022, **13**, 6064.
[16] D. Shen, A. M. Rao, J. Zhou and B. Lu, *Angew. Chem., Int. Ed.*, 2022, **61**, e202201972.
[17] W. Song, J. Zhang, C. Wen, H. Lu, C. Han, L. Xu and L. Mai, *J. Am. Chem. Soc.*, 2024, **146**, 4762–4770.
[18] F. Meng, X. Dong, H. Wu, Z. Wu, H. Dou and X. Zhang, *Adv. Funct. Mater.*, 2025, **35**, 2422079.
[19] Z. Li, Y. Lin, J. Ruan, M. Liao, F. Wang, R. Jiang, X. Qu, Q. Li, J. Yang, X. Li, Z. Zhang, Y. Li, D. Sun, F. Fang and F. Wang, *Angew. Chem., Int. Ed.*, 2025, **64**, e202416800.
[20] Z. Zhu, W. Wang, Y. Yin, Y. Meng, Z. Liu, T. Jiang, Q. Peng, J. Sun and W. Chen, *J. Am. Chem. Soc.*, 2021, **143**, 20302–20308.
[21] Y. Liu, Y. Liu, X. Chen, X. Cui, J. Chen, Y. Cao, G. Li, Y. Feng, F. Jiang, M. Liao and Y. Wang, *Adv. Funct. Mater.*, 2025, **35**, 202510648.
[22] S. Chandra, D. Roy Chowdhury, M. Addicoat, T. Heine, A. Paul and R. Banerjee, *Chem. Mater.*, 2017, **29**, 2074–2080.
[23] S. Brahma and K. Ramanujam, *Ionics*, 2022, **28**, 1427–1440.
[24] A. M. Khattak, Z. A. Ghazi, B. Liang, N. A. Khan, A. Iqbal, L. Li and Z. Tang, *J. Mater. Chem. A*, 2016, **4**, 16312–16317.
[25] F. Yue, Z. Tie, S. Deng, S. Wang, M. Yang and Z. Niu, *Angew. Chem., Int. Ed.*, 2021, **60**, 13882–13886.
[26] R. B. Rakhi and M. L. Lekshmi, *Electrochim. Acta*, 2017, **231**, 539–548.
[27] Y. Liao, H. Wang, M. Zhu and A. Thomas, *Adv. Mater.*, 2018, **30**, 1705710.
[28] N. An, Y. An, Z. Hu, Y. Zhang, Y. Yang, Z. Lei, *RSC Adv.*, 2015, **5**, 63624–63633.
[29] D. P. Dubal, N. R. Chodankar, Z. Caban-Huertas, F. Wolfart, M. Vidotti, R. Holze, C. D. Lokhande and P. Gomez-Romero, *J. Power Sources*, 2016, **308**, 158–165.